Molecular transport across fluid interfaces: Coupling between solute dynamics and interface fluctuations

Ashish Gupta, Anuj Chauhan, and Dmitry I. Kopelevich
Department of Chemical Engineering, University of Florida, Gainesville, Florida 32611-6005, USA
(Received 1 August 2008; published 13 October 2008)

We investigate the transport mechanism of a small hydrophobic solute molecule across two types of fluid interfaces, (i) an interface between two immiscible liquids and (ii) a surfactant-covered liquid-liquid interface. These systems are modeled by coarse-grained molecular dynamics simulations. It is demonstrated that the dynamics of the solute molecule near the interface significantly deviates from Markovian Brownian motion. Specifically, the correlation time of the random force acting on the solute strongly depends on the distance between the solute and the interface and increases by two orders of magnitude within a very narrow (less than 1 nm wide) region near the interface. The slow fluctuations of the random force in this narrow region are caused by capillary waves. The region location and width are determined by interface protrusions caused by attraction between the solute and the hydrophobic phase. We use results of molecular dynamics simulations to develop a stochastic model for the coupled solute-interface dynamics and estimate the rate of the solute transport across the interface. The observed phenomenon appears to be a general feature of mass transport across fluid or flexible membranes. The coupling between the solute transport and the interface fluctuations is the strongest in areas corresponding to a large free energy gradient or near a free energy barrier for the solute transport. This suggests a strong influence of the coupled solute-interface dynamics on the rate of mass transfer across interfaces.

DOI: 10.1103/PhysRevE.78.041605 PACS number(s): 68.05.Gh, 05.40.−a, 66.10.cg, 68.03.Kn

I. INTRODUCTION

The process of mass transfer across an interface between two immiscible liquids or a flexible membrane of molecular thickness, such as a surfactant-covered liquid-liquid interface, plays a key role in numerous applications, including separations, reactions, and drug delivery [1–4]. Molecular transport across an interface of two immiscible fluids is a subject of active experimental [5–8], computational [9–18], and theoretical [19–21] studies.

It may seem intuitive that transport of a simple solute, such as a spherical molecule or an ion, can be reduced to dynamics of a single degree of freedom, namely the distance z between the solute and the interface. In this case, the role of the solvents in the solute transport would reduce to that of (i) mean force $F(z)$ which depends only on z and acts on the solute as it traverses the interface and (ii) thermal collisions between the solute and solvent molecules resulting in a Markovian random force acting on the solute. However, starting with the pioneering work of Benjamin and co-workers [9,11], it has become apparent that, at least in the case of an ion transport across a fluid-fluid interface, solvents actively participate in the transport process and their role cannot be reduced to that of the mean force $F(z)$ and the thermal noise. Molecular dynamics (MD) simulations [9,11] of an ion transfer across a water/1,2-dichloroethane interface demonstrated formation of short-lived (with lifetime on the order of tens of picoseconds) capillary fingers of solvent protruding toward the solute when the latter is located close to the dividing surface. Formation of such protrusions during transport of an ion across an interface between two immiscible liquids has been confirmed by MD simulations for multiple ion-solvent systems [15–17,22–24]. Evidence of importance of capillary waves in transport across an interface has also been observed experimentally [6].

Based on these observations, several models of the coupled solute-solvent dynamics have been proposed. In one of the early models [19], ion transport across an interface is assumed to be initiated by a solute capture by an interface protrusion and proceeds through a sequence of activated exchanges of molecules inside the solute solvation shell. Kornyshev *et al.* [20] extended this idea and proposed a model which, in addition to effects of the fluctuation-induced interface protrusion on the solute transport, captures the feedback effect of the solute on the protrusion formation. In this model for the coupled solute-interface dynamics the interface is described by a single degree of freedom, namely the height of the protrusion, and other degrees of freedom of the interface are neglected. Despite this approximation, it allows one to qualitatively assess effects of the coupled surface-solute dynamics on the solute transport. It is demonstrated that, in the case of a relatively small energy barrier for transport across the interface, the capillary fluctuations slow down the solute transport. A further extension of this model which explicitly accounts for all modes of the interface fluctuations was proposed by Daikhin *et al.* [21]. Since the main focus of the latter work was to assess the interface fluctuations in the presence of ions, the authors did not present estimates of the ion transport rate based on this improved model.

The above observations and models for the coupled solute-interface dynamics were made for a charged solute in a system containing at least one polar or electrolyte solvent. In the current paper, we demonstrate that the solute transport may be coupled to the interface fluctuations even in the absence of long-range electrostatic interactions. We use coarse-grained MD simulations to investigate transport of a small nonionic solute across (i) an oil-water interface and (ii) a monolayer of nonionic surfactants adsorbed at an oil-water interface. In both considered systems, the solute-interface

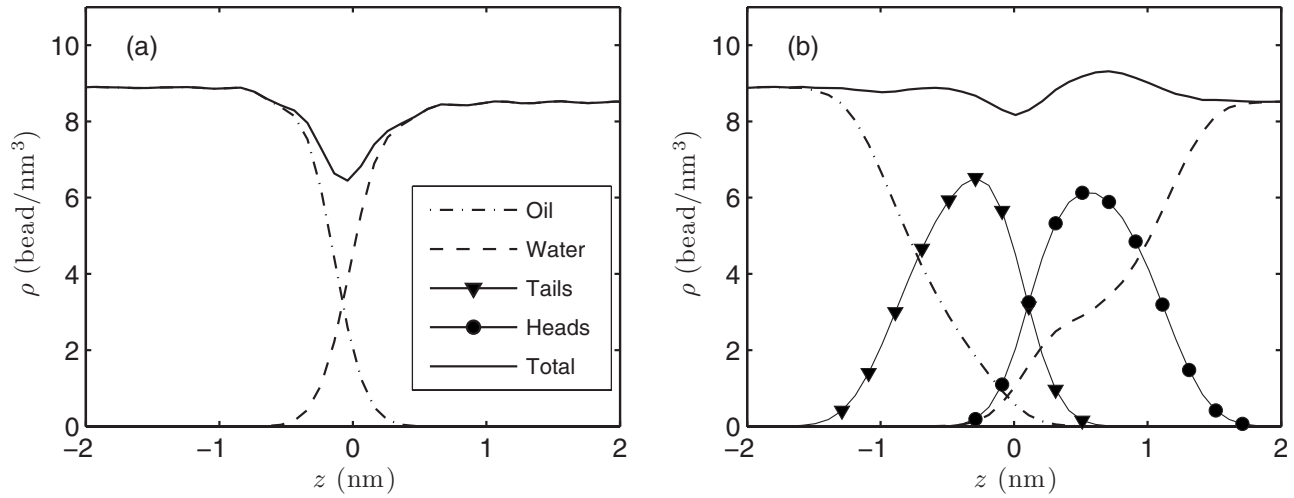

FIG. 1. Density profiles of (a) surfactant-free hexadecane-water interface and (b) hexadecane-water interface covered by H_3T_3 surfactants [26].

coupling leads to a locally non-Markovian stochastic force acting on the solute. The correlation time of the stochastic force significantly increases (by as much as two orders of magnitude) when the solute is located near a free energy barrier or in a region corresponding to a large free energy gradient. Therefore, detailed understanding of the origin of this position dependence of the fluctuation time scales is necessary to correctly predict rates of mass transfer across interfaces. We show that coupling of the solute motion with relatively slow hydrodynamic and, if applicable, elastic interface fluctuations is facilitated by a local deformation of the interface caused by the presence of the solute. We use MD results to develop a stochastic model for the coupled interface-solute dynamics and show that it is similar to the phenomenological model for ion transport proposed by Daikhin *et al.* [21]. Finally, we discuss effects of this coupling on the solute transport rate and discuss implications of the slow fluctuations on the analysis of MD simulations of interfacial systems.

II. MODEL AND SIMULATION DETAILS

The studies are performed using a coarse-grained molecular dynamics (CGMD) model proposed by Marrink *et al.* [25]. This model is shown to yield good agreement with experiments and atomistically detailed simulations for a wide range of molecular systems and, in particular, can accurately reproduce densities and mutual solubilities of water and alkanes [25], as well as the interfacial tension at an oil-water interface [26]. In our recent work [26,27] we extended this model to include a model for nonionic ethoxylated surfactants C_iEO_j. For the sake of completeness, below we briefly review salient features of the model.

All molecules in the systems considered in the current work are modeled using two types of beads: Hydrophobic tail bead (denoted here as T) and hydrophilic head bead (denoted as H). A single tail bead approximates four methyl or methylene groups in alkane chains and a single head bead approximates four water molecules [25] or two ethoxy groups [26,27]. Interactions between nonbonded beads are modeled by the Lennard-Jones (LJ) potential. All beads have the same LJ diameter, σ=0.47 nm, and the hydrophobic or hydrophilic nature of a bead is modeled by the strength ϵ of the LJ potential. In the current work, we consider transport of a small spherical solute modeled by a tail bead T across (i) water-hexadecane interface and (ii) water-hexadecane interface covered by H_3T_3 ($\approx C_{12}EO_6$) surfactants.

MD simulations are performed using the GROMACS package [28]. The Verlet integration scheme is used with a time step of 0.04 ps. The temperature and pressure are kept constant at 300 K and 1 bar. Unless stated otherwise, we use Berendsen temperature and isotropic pressure coupling schemes [29] with time constant 1 ps and compressibility 10^{-5} bar^{-1} in the pressure coupling scheme.

The simulations are performed in a cubic cell with a side of 10 nm. The interfaces are prepared by simulations of self-assembly of mixtures of oil, water, and, if applicable, surfactant molecules with nearly equal mass fractions of oil and water [26]. Density profiles of equilibrated interfaces are shown in Fig. 1. The system of coordinates is oriented so that the z axis is normal to the interface, the positive direction of the z axis points to the water phase, and the x-y plane corresponds to the dividing surface of the interface in the absence of the solute. In the remainder of this paper, this surface will be referred to as the neutral surface (or plane) in order to distinguish it from dividing surfaces perturbed by interactions with the solute.

In order to analyze interface fluctuations, it is necessary to define a procedure to obtain space- and time-dependent dividing surfaces from molecular-level information. This can be accomplished, for example, by a generalization of the Gibbs dividing surface based on local averaging of fluid density profiles [30]. However, this approach does not provide sufficient separation between the interface and bulk degrees of freedom at small length scales [31,32]. Therefore, we follow Refs. [31–33] and use a definition of the position-dependent instantaneous dividing surface tied directly with locations of molecules at the interface. The location of the neutral plane is then obtained by averaging of the instanta-

neous dividing surfaces in the absence of the solute.

The instantaneous dividing surface $z=h(x,y;t)$ at time t is determined from a set of pivot points (x_j,y_j,z_j) obtained from the molecular configuration at time t. For the surfactant-covered interfaces, the pivot points correspond to midpoints of bonds connecting the tail and head groups of surfactant molecules. The pivot points for the surfactant-free oil-water interface are determined following an approach similar to that used in Refs. [31–33]. For each water bead, we define a pivot point as a location of an oil bead closest to it. The surface defined by these pivot points is referred to as the oil surface. Similarly, we define pivot points of the water surface as a collection of water beads closest to oil beads. Properties of the oil and water surfaces relevant to the current study are the same. Therefore, in this paper we report results obtained for the water surface.

In what follows, we will need to analyze continuous approximations to and Fourier transforms of the instantaneous dividing surfaces. Instantaneous Fourier harmonics $\hat{h}_{\mathbf{k}}(t)$ are obtained by a least squares fit of the instantaneous dividing surface to truncated Fourier series,

$$\sum_j |z_j(t) - h(x_j(t),y_j(t);t)|^2 \to \min, \tag{1}$$

where

$$h(x,y;t) = \sum_{|\mathbf{k}|\le k_{\mathrm{cut}}} \hat{h}_{\mathbf{k}}(t) e^{i(k_x x + k_y y)} \tag{2}$$

is the continuous instantaneous dividing surface defined by the pivot points. In Eq. (2) $\mathbf{k}=(k_x,k_y)$ is a wave vector and $k_{\mathrm{cut}}=2\pi$ nm^{-1} is the cutoff wave-vector magnitude which approximately corresponds to two diameters of the coarse-grained beads.

III. GENERALIZED LANGEVIN MODEL FOR A SINGLE REACTION COORDINATE

We assume that the solute transport can be described by a generalized Langevin equation,

$$m\ddot{z}_s + \int_{-\infty}^{t} \gamma(t-\tau;z_s)\dot{z}_s(\tau)d\tau + \frac{dG(z_s)}{dz_s} = \Gamma(t;z_s). \tag{3}$$

In this equation, z_s is the distance between the solute and the neutral interface, m is the mass of the solute, $G(z_s)$ is the free energy or the potential of mean force, $\gamma(t;z_s)$ is the memory friction kernel, and $\Gamma(t;z_s)$ is the random force with Gaussian distribution and zero mean. The autocorrelation function (ACF) $C(t;z_s)$ of $\Gamma(t;z_s)$ is related to the friction kernel $\gamma(t;z_s)$ by the fluctuation-dissipation theorem [34–36],

$$C(\tau;z_s) \equiv \langle \Gamma(t;z_s)\Gamma(t+\tau;z_s)\rangle = k_B T \gamma(\tau;z_s). \tag{4}$$

The gradient of the free energy $G'(z_s)$ and the friction kernel γ are obtained using constrained MD simulations [34,35]. A natural choice of a reaction coordinate is the solute coordinate z_s, i.e., the distance between the solute and the neutral dividing surface. However, this choice is not very convenient for constrained MD simulations, since in this case the constraint would involve a quantity averaged over time, whereas algorithms for constrained simulations typically deal with instantaneous system configurations. Therefore, in our simulations we constrain the distance ζ_s between the solute and the instantaneous center of mass of a segment of either the oil phase (for the surfactant-free interface) or the surfactant monolayer (for the surfactant-covered interface) contained in the simulation box. Since fluctuations of the locations of these centers of mass are negligible, the results obtained by constraining ζ_s are equivalent to those that would have been obtained by constraining z_s. Therefore, for convenience, in the following discussion we will refer to z_s as the constrained variable.

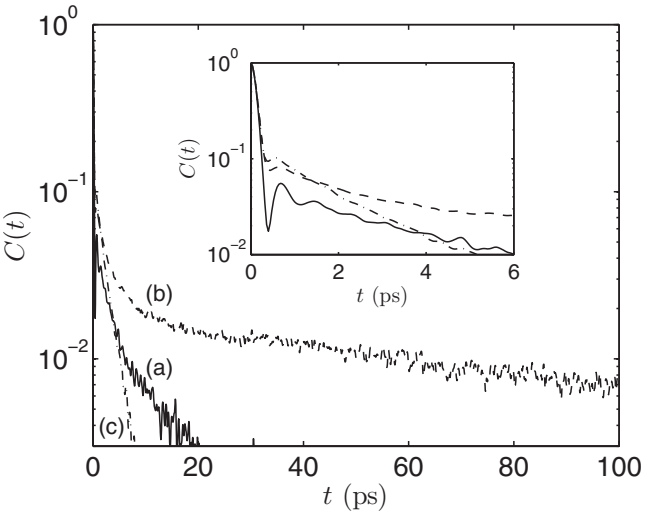

FIG. 2. ACF of the random force $\Gamma(t;z_s)$ acting on the solute near the surfactant-free oil-water interface. In this plot, ACF are normalized so that $C(t=0;z_s)=1$. The solute is constrained at (a) $z_s=-1.06$ nm (solid line), (b) $z_s=0.59$ nm (dashed line), and (c) $z_s=1.75$ nm (dashed-dotted line). The inset shows $C(t;z_s)$ for small t.

Initial conditions for the constrained simulations were prepared by pulling the solute molecule across the interface by applying an artificial force. The solute was then constrained using the SHAKE algorithm [37] and the system was equilibrated for 10 ns. This was followed by a 390 ns production run for surfactant-free systems and a 490 ns production run for systems containing H_3T_3 monolayers.

The mean of the constraining force F_z acting on the solute corresponds to the gradient of the potential of mean force,

$$\langle F_z\rangle = \frac{dG(z_s)}{dz_s}, \tag{5}$$

and the deviations of F_z from its mean correspond to the random force acting on the solute,

$$\Gamma(t,z_s) = F_z(t,z_s) - \langle F_z(z_s)\rangle. \tag{6}$$

We observe that time scales of fluctuations of $\Gamma(t,z_s)$ are extremely sensitive to the distance z_s between the solute and the neutral dividing surface, as illustrated by examples of the force ACF $C(t;z_s)$ shown in Fig. 2. The force fluctuations have large correlation time when the solute is located at $z_s=0.59$ nm while in the other two shown examples the corre-

lation time is very small. In order to confirm that the observed large correlation time of the random force represents a real physical phenomenon and is not due to an artifact of a particular method of constraining temperature, pressure, or solute position used in MD simulations, we perform additional simulations with (1) weak Berendsen temperature and pressure coupling (time constant 100 ps), (2) a Nosé-Hoover thermostat [38,39] with time constant 1 ps and a Parrinello-Rahman barostat [40,41] with time constant 5 ps, and (3) a constraint on the solute position implemented via assignment of zero solute velocity in the z_s direction at each MD step. The considered alternative simulation methods produced the same results, thus confirming that the slow random force fluctuations are real.

Figure 2 indicates that, after fast initial oscillations (for $t \leqslant 2$ ps), the decay of the force ACF follows either a single or a double exponential law:

$$C(t;z_s) = C_1(z_s)e^{-t/\tau_1(z_s)} \tag{7}$$

or

$$C(t;z_s) = C_1(z_s)e^{-t/\tau_1(z_s)} + C_2(z_s)e^{-t/\tau_2(z_s)}, \quad \tau_1(z_s) < \tau_2(z_s), \tag{8}$$

depending on the solute location. The fast decay time, τ_1, is always small ($\leqslant 15$ ps), whereas the slow decay time, τ_2, is extremely sensitive to the solute location, as can be seen from Fig. 3(a). In this figure, we plot $\tau_f(z_s)$, which is defined as $\tau_1(z_s)$ if Eq. (7) holds and $\tau_2(z_s)$ if Eq. (8) holds for the solute constrained at $z=z_s$. The decay time $\tau_f(z_s)$ varies by two orders of magnitude in a narrow region near the interface. From the free energy profiles shown in Fig. 3(b) it is evident that the slow force fluctuations take place either in a region with a steep free energy gradient (at the surfactant-free interface) or near a free energy barrier (at the surfactant-covered interface). Therefore, the observed inhomogeneity in the force correlation times is expected to impact the solute transport across the interface.

The fluctuations of the force acting on the solute are directly related to fluctuations of the solvent and, if applicable, surfactant density near the solute. The fast density fluctuations correspond to diffusive motion of individual particles, whereas the slow density fluctuations correspond to capillary waves at the interface. Interestingly, the slow force fluctuations are observed only on one side of the interface while the interface fluctuations are expected to cause slow density fluctuations on both sides of the dividing surface.

This asymmetry of the force fluctuations is caused by an attractive interaction between the solute and the hydrophobic phase. Effects of this attractive force on the surfactant-free oil-water interface and H_3T_3 monolayer are illustrated in Figs. 4(a) and 4(b), respectively. The averaged dividing surfaces $z=h^{(0)}(r;z_s)$ shown in these figures are obtained from MD simulations with the solute constrained at $z=z_s$. Here, r denotes the distance between a point on the neutral plane and the solute projection onto this plane.

Figures 4(a) and 4(b) show averaged dividing surfaces $z=h^{(0)}(r,z_s)$ corresponding to four representative solute positions, $z_s=z_i$, $i=1,\ldots,4$; $z_1<z_2<z_3<z_4$. The average dividing surface remains unperturbed when the solute is located in the oil-rich phase, even if the solute is relatively close to the neutral surface, as illustrated by $h^{(0)}(r;z_s=z_1)$. As the solute approaches the neutral plane, it starts pushing the interface toward the water-rich phase; see $h^{(0)}(r;z_s=z_2)$. The interface deforms in order to maximize wetting of the solute by hydrophobic groups and to minimize the solute interactions with hydrophilic groups. As the solute crosses the dividing surface and moves into the water-rich phase, the protrusion into this phase grows due to attraction between the solute and hydrophobic groups located on the opposite side of the interface. The protrusion height reaches its maximum when $z_s \approx z_3$. Further solute displacement into the water-rich phase requires a larger interface deformation to ensure that the hydrophobic groups are within the interaction range of the solute. Eventually, an increase of the interfacial energy due to such deformations becomes too large to be compensated by the favorable interactions of the solute with the hydrophobic groups. Therefore, once the solute passes through the point corresponding to the maximum protrusion height, the protru-

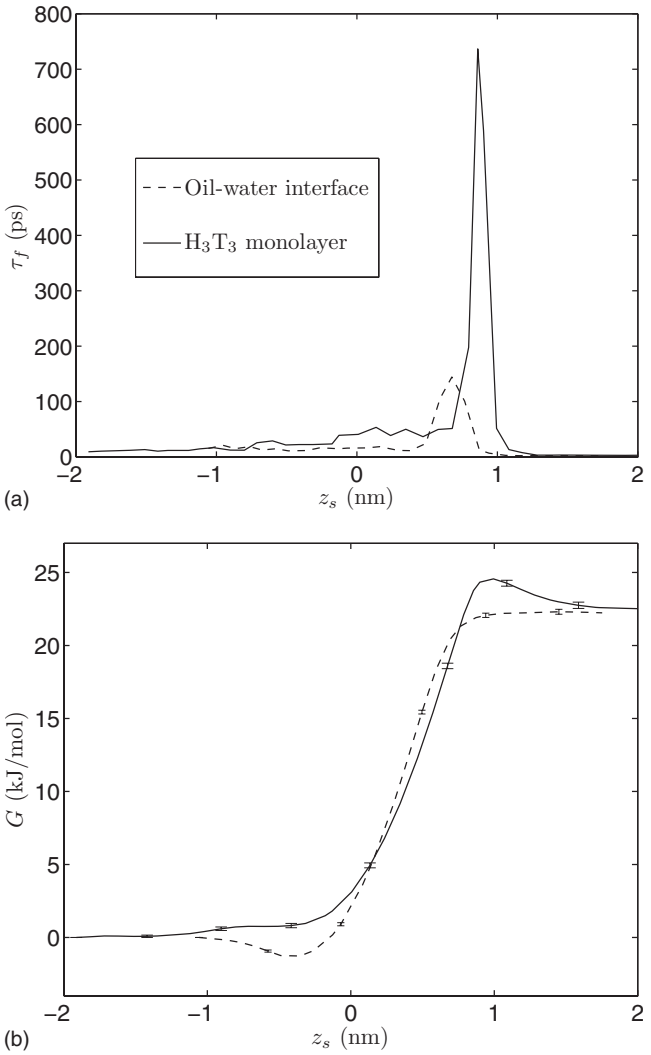

FIG. 3. (a) Correlation time $\tau_f(z_s)$ of the slowest fluctuations of the random force $\Gamma(z_s;t)$ acting on the solute constrained at $z=z_s$ near surfactant-free and surfactant-covered interfaces; (b) corresponding free energy profiles.

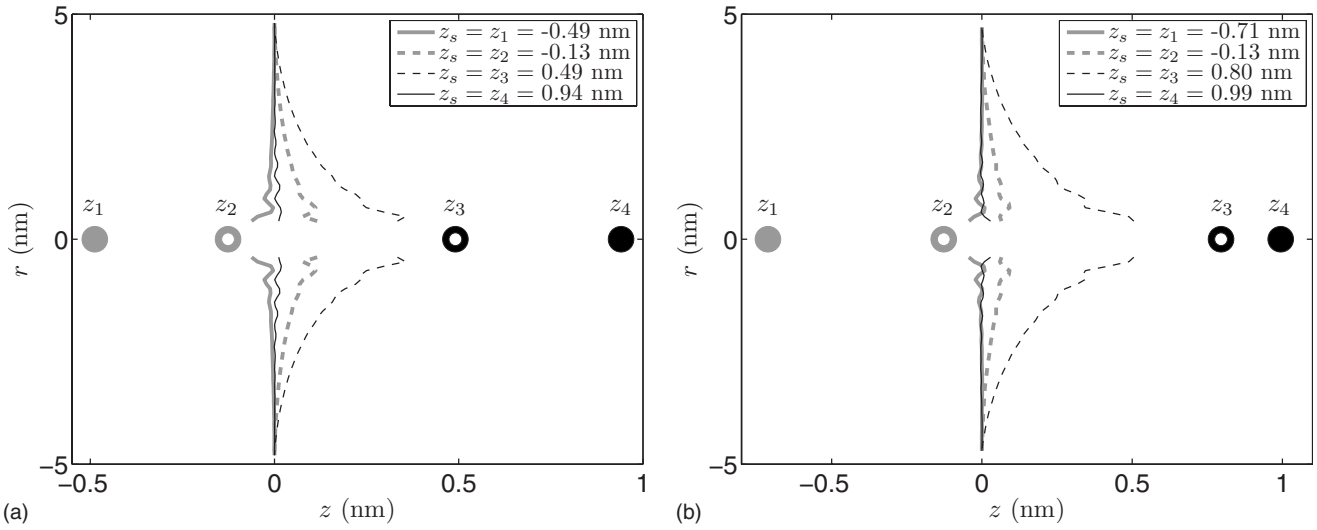

FIG. 4. Average dividing surfaces $z=h^{(0)}(r;z_s)$ corresponding to the solute constrained at different $z=z_s$ near the (a) surfactant-free oil-water interface and (b) H_3T_3 monolayer. To emphasize rotational symmetry of the dividing surfaces, symmetric reflections of these surfaces with respect to the z axis are also plotted. Dividing surfaces exhibiting significant deviations from the unperturbed planar interface are shown by dashed lines and the corresponding solute locations are shown by hollow circles. Solute locations which do not lead to significant interface perturbations are indicated by filled circles and the corresponding dividing surfaces are shown by solid lines. The gray (black) lines and circles correspond to solute located on the oil- (water-) rich sides of the interface.

sion disappears fairly quickly and the interface returns to its unperturbed state when $z_s \approx z_4$.

The strong dependence of the average interface shape on the solute position is a key factor leading to the slow fluctuations of the random force $\Gamma(z_s;t)$. To see this, consider a solute-interface system with the solute constrained at some $z_s=z_0$. In this system, the dividing surface fluctuates around its average $h^{(0)}(r;z_0)$. Remove the constraint at time t_0 and consider the system configuration at time $t_1=t_0+\Delta t$, where Δt is on the order of the time scale τ_1 of the fast fluctuations of $\Gamma(z_s;t)$. Assume that a small solute displacement in the z direction which happened between t_0 and t_1 corresponds to a substantial change of the average interface shape. In this case, the instantaneous interface shape at time t_1 will be different from the average shape $h^{(0)}(r;z_s(t_1))$, since the time scale of the interface relaxation is much larger than the time scale τ_1 of the fast fluctuations of $\Gamma(z_s;t)$. The unfavorable interface configuration caused by its delayed response will lead to a strong restoring force pulling the solute back toward $z=z_0$. This force corresponds to the slow component of the force $\Gamma(z_s;t)$ and its time scale corresponds to the interface relaxation time. As will be demonstrated in the next section, this relaxation time is on the order of hundreds of picoseconds, which is consistent with the time scale of the slow component of $\Gamma(z_s;t)$ in the region of the strong solute-interface coupling.

This restoring force will be especially strong in regions corresponding to the large gradient of $h^{(0)}(r;z_s)$ with respect to z_s, such as the region between points z_3 and z_4 in Fig. 4. In such regions, a small solute displacement causes a large change in the average protrusion magnitude and hence a strong restoring force. In the following section, we develop a stochastic model for the coupled solute-interface dynamics and demonstrate that the above qualitative arguments are consistent with the predictions of this more detailed model.

IV. MODEL FOR COUPLED SOLUTE-INTERFACE DYNAMICS

We assume that interactions between the solute and its surroundings can be described by the potential $G(z_s;\{\hat{h}_\mathbf{k}\})$ of mean force acting between the solute located at $z=z_s$ and the interface in the configuration defined by Fourier coefficients $\{\hat{h}_\mathbf{k}\}$. In this model we neglect details of the microstructure of the interface and assume that this microstructure can be adequately modeled by its contributions to (i) the potential of mean force and (ii) Markovian random forces acting on the solute and the interface. In what follows we use a moving system of coordinates with the origin corresponding to the solute projection on the neutral dividing surface.

In order to obtain information regarding the mean and stochastic forces acting on the interface modes $\{\hat{h}_\mathbf{k}\}$, we consider dynamics of $\hat{h}_\mathbf{k}(t)$ when the solute is constrained at various positions z_s. Typical examples of ACF $C_\mathbf{k}(\tau;z_s)$ of the interface modes $\hat{h}_\mathbf{k}(t)$ are shown in Fig. 5. For all considered solute positions z_s, it is observed that $C_\mathbf{k}(\tau;z_s)$ can be adequately approximated by exponentials and correlations between different modes are negligible, i.e.,

$$\langle \xi_\mathbf{k}(t)\xi^*_\mathbf{m}(t+\tau)\rangle|_{z_s=\text{const}} = \delta_{\mathbf{km}} D_\mathbf{k}(z_s) e^{-\tau/\tau_\mathbf{k}(z_s)}, \quad \mathbf{k},\mathbf{m} \neq 0. \tag{9}$$

Here,

$$\xi_\mathbf{k}(t,z_s) \equiv \hat{h}_\mathbf{k}(t) - \hat{h}^{(0)}_\mathbf{k}(z_s) \tag{10}$$

is a deviation of the interface mode $\hat{h}_\mathbf{k}$ from its average value $\hat{h}^{(0)}_\mathbf{k}(z_s)$.

Equation (9) implies that all $\xi_\mathbf{k}$ undergo independent Markovian Ornstein-Uhlenbeck processes [42],

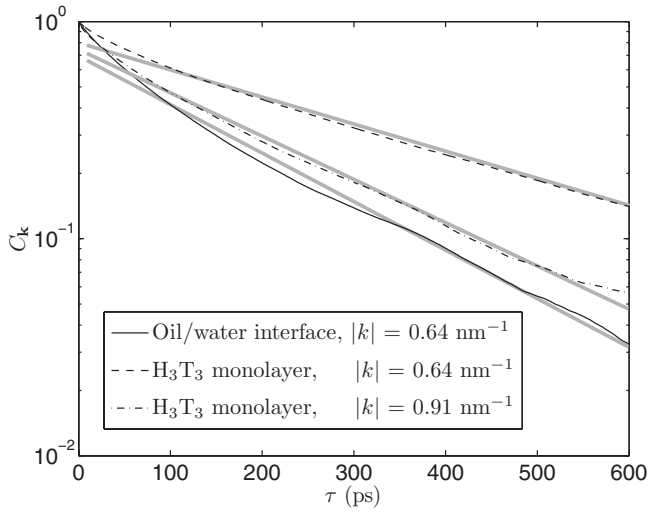

FIG. 5. Examples of ACF $C_{\mathbf{k}}(\tau;z_s)$ of the interface modes for the surfactant-free oil-water interface (z_s=0.59 nm) and H_3T_3 monolayer (z_s=0.67 nm). Thick gray lines show exponential fits to $C_{\mathbf{k}}(\tau;z_s)$. In this plot, ACF are normalized so that $C_{\mathbf{k}}(\tau=0;z_s)=1$.

$$\gamma_{\mathbf{k}}(z_s)\frac{d\xi_{\mathbf{k}}}{dt} = -\alpha_{\mathbf{k}}(z_s)\xi_{\mathbf{k}} + \Gamma_{\mathbf{k}}(t), \quad \mathbf{k} \neq 0, \quad z_s = \text{const}, \tag{11}$$

where

$$\alpha_{\mathbf{k}} = \frac{k_B T}{\langle|\xi_{\mathbf{k}}|^2\rangle} > 0 \quad \text{and} \quad \gamma_{\mathbf{k}} = \alpha_{\mathbf{k}}\tau_{\mathbf{k}} > 0. \tag{12}$$

The friction coefficient $\gamma_{\mathbf{k}}$ and the stochastic force $\Gamma_{\mathbf{k}}(t)$ satisfy the fluctuation-dissipation theorem,

$$\langle\Gamma_{\mathbf{k}}(t)\Gamma^*_{\mathbf{m}}(s)\rangle|_{z_s=\text{const}} = 2k_B T\gamma_{\mathbf{k}}(z_s)\delta_{\mathbf{km}}\delta(t-s), \quad \mathbf{k},\mathbf{m} \neq 0. \tag{13}$$

The equation for $\hat{h}_{\mathbf{k}}$ follows directly from Eqs. (10) and (11):

$$\gamma_{\mathbf{k}}(z_s)\frac{d\hat{h}_{\mathbf{k}}}{dt} = -\alpha_{\mathbf{k}}(z_s)[\hat{h}_{\mathbf{k}} - \hat{h}^{(0)}_{\mathbf{k}}(z_s)] + \Gamma_{\mathbf{k}}(t), \quad \mathbf{k} \neq 0. \tag{14}$$

The deterministic component of the right-hand side of Eq. (11) corresponds to the negative derivative of the potential of mean force $G(z_s;\{\hat{h}_{\mathbf{k}}\})$ with respect to $\hat{h}^*_{\mathbf{k}}$, which implies that

$$G(z_s;\{\hat{h}_{\mathbf{k}}\}) = G_0(z_s) + \frac{1}{2}\sum_{\mathbf{k}\neq 0}\alpha_{\mathbf{k}}(z_s)|\hat{h}_{\mathbf{k}} - \hat{h}^{(0)}_{\mathbf{k}}(z_s)|^2, \tag{15}$$

where function $G_0(z_s)$ is independent of the interface shape. The sum in the right-hand side of Eq. (15) is finite due to natural cutoff values for magnitudes of the wave vectors $\mathbf{k}$; due to gravity and/or failure of the linear capillary wave model for long waves (i.e., small $|k|$) and due to finite molecular size for short waves (large $|k|$).

Although Eq. (14) was obtained for z_s=const, this equation is likely to remain valid even if the solute is not constrained. To see this, assume that Eq. (14) contains an additional term which vanishes if z_s is kept constant. If this term contributes to the deterministic component of Eq. (14), it corresponds to a time derivative of some function $f(z_s)$ of z_s, i.e., it is proportional to the solute velocity $\dot{z}_s$. Since this term would have to be contained in the derivative of the potential of mean force with respect to $\hat{h}^*_{\mathbf{k}}$ and, according to our earlier assumption, $G(z_s;\{\hat{h}_{\mathbf{k}}\})$ is independent of $\dot{z}_s$, it follows that $f \equiv 0$ and the deterministic component of Eq. (14) remains valid for an unconstrained solute. Moreover, it is unlikely that the stochastic component of Eq. (14) contains any additional terms vanishing if z_s=const, since it is unlikely that the stochastic force acting on the interface depends on the solute velocity $\dot{z}_s$. Therefore, in what follows we assume that the interface modes satisfy Eq. (14) even if the solute is not constrained.

From Eq. (15) it follows that the solute dynamics is described by the following Langevin equation:

$$m\frac{d^2 z_s}{dt^2} + \gamma_s(z_s)\frac{dz_s}{dt} = -G_0'(z_s) - \frac{1}{2}\frac{d}{dz_s}\left(\sum_{\mathbf{k}\neq 0}\alpha_{\mathbf{k}}(z_s)|\hat{h}_{\mathbf{k}} - \hat{h}^{(0)}_{\mathbf{k}}(z_s)|^2\right) + \Gamma_s(t;z_s), \tag{16}$$

where $\Gamma_s(t;z_s)$ is the Markovian random force due to interactions of the solute with individual solvent and surfactant molecules. $\Gamma_s(t;z_s)$ is independent from the random forces $\Gamma_{\mathbf{k}}(t)$ acting on the interface modes and satisfies the fluctuation-dissipation theorem,

$$\langle\Gamma_s(t;z_s)\Gamma_s(s;z_s)\rangle = 2k_B T\gamma_s(z_s)\delta(t-s). \tag{17}$$

The second term on the right-hand side of Eq. (16) represents the contribution of the interface fluctuations to the force acting on the solute. This contribution is significant if $\alpha_{\mathbf{k}}(z_s)$ or $\hat{h}^{(0)}_{\mathbf{k}}(z_s)$ exhibit strong dependence on z_s. In this case, the time scale of the force fluctuations is determined by the time scales $\tau_{\mathbf{k}}(z_s)$ of the corresponding interface modes. Dependence of $\hat{h}^{(0)}_{\mathbf{k}}$, $\alpha_{\mathbf{k}}$, and $\tau_{\mathbf{k}}$ on z_s for one of the interface modes is shown in Fig. 6. As can be seen, $\hat{h}^{(0)}_{\mathbf{k}}$ exhibits strong dependence on the solute position due to protrusions formed at the interface in the presence of the solute. The gradient of $\hat{h}^{(0)}_{\mathbf{k}}(z_s)$ is much larger on the hydrophilic side of the interface, in agreement with the physical picture of attraction between the solute and the hydrophobic beads. Equation (16) then implies that the contribution of the interface fluctuations to the solute dynamics is significant only on the water side of the interface, which is consistent with the observation that the random force fluctuations are slow only on one side of the interface (see Fig. 3). Moreover, the gradient of $\hat{h}^{(0)}_{\mathbf{k}}(z_s)$ is the largest for z_s corresponding to the peaks of the force correlation time $\tau_f(z_s)$.

The sharp decrease of $\hat{h}^{(0)}_{\mathbf{k}}(z_s)$ is caused by disappearance of the interface protrusions once the energy of their attraction to the solute becomes smaller than the increase of the interfacial tension caused by the protrusion formation. Therefore,

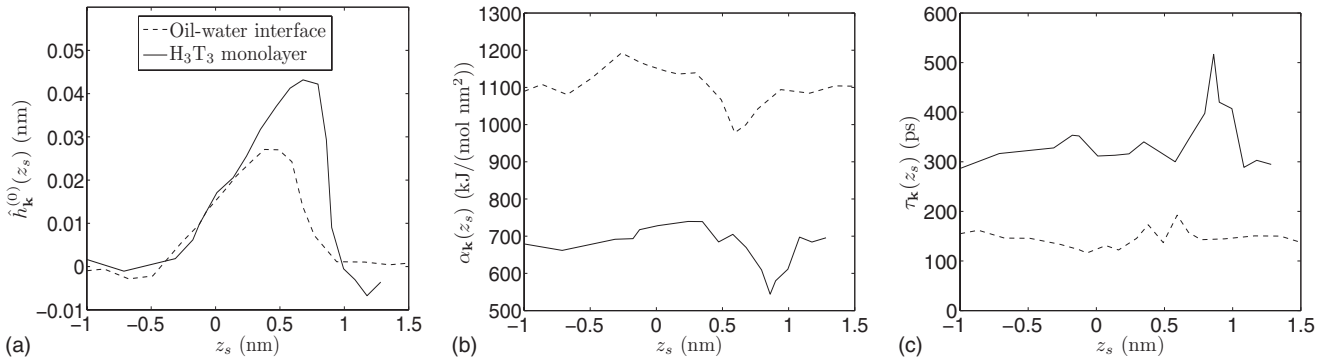

FIG. 6. Dependence of (a) $\hat{h}_{\mathbf{k}}^{(0)}$, (b) $\alpha_{\mathbf{k}}$, and (c) $\tau_{\mathbf{k}}$ on z_s for a wave vector $\mathbf{k}$ with magnitude 0.64 nm^{-1}.

Eq. (16) confirms the qualitative arguments presented in Sec. III relating the slow force fluctuations with the strong dependence of the interface shape on the solute location. The time scale of the interface relaxation estimated from Fig. 6(c) is consistent with the time scale of the slow component of the random force acting on the solute, thus further supporting these arguments. The location and the width of the region with large $\tau_f(z_s)$ and large gradient of $\hat{h}_{\mathbf{k}}^{(0)}(z_s)$ are primarily determined by relative magnitudes of the interfacial energy and the energy of attraction between the solute and the hydrophobic phase. As Figs. 6(b) and 6(c) indicate, presence of the solute in the region of the large gradient of $\hat{h}_{\mathbf{k}}^{(0)}(z_s)$ also lead to a small decrease of $\alpha_{\mathbf{k}}(z_s)$ (i.e., an increase of the fluctuation magnitude) and an increase of the correlation time $\tau_{\mathbf{k}}$ of the interface modes. The latter effect is especially pronounced for the surfactant monolayer.

V. DISCUSSION

The obtained equations (14) and (16) for the coupled solute-interface dynamics are similar to the model proposed by Daikhin *et al.* [21] for coupling between an ion and an electrolyte interface. In the current work, we demonstrated that this model is valid for nonionic fluid-fluid and surfactant-covered interfaces. Moreover, this model is directly verified by and its parameters are obtained from MD simulations, which enables quantitative predictions of the solute transport rates. In addition, it is observed that even a small solute may significantly influence the time scale of fluctuations of a surfactant monolayer; see Fig. 6(c).

In conclusion, we discuss an impact of the solute-interface coupling on analysis of constrained MD simulations and the solute transport rate. Equations (14) and (16) imply that in the regions of strong solute-interface coupling, random force $\Gamma_{\mathrm{MD}}(t;z_s)$ obtained from constrained MD simulations corresponds to a combination of a thermal Markovian force $\Gamma_s(t;z_s)$ and a contribution from the interface fluctuations. In these regions, the solute friction coefficient $\gamma_s(z_s)$ should be computed from Eq. (4) using the ACF of Γ_s and not that of Γ_{MD}. In Fig. 7, we show a comparison of the friction coefficients $\gamma_{\mathrm{MD}}(z_s)$ and $\gamma_s(z_s)$ obtained from the ACF of Γ_{MD} and Γ_s, respectively. For the solute positions z_s corresponding to strong solute-interface coupling, the ACF of Γ_s was estimated by removing the slowly decaying component [i.e., the second exponential term in Eq. (8)] from the ACF of Γ_{MD}. For all other z_s, $\Gamma_s(t;z_s)$ is assumed to be identical to $\Gamma_{\mathrm{MD}}(t;z_s)$.

Figure 7 indicates that the solute-interface coupling is responsible for a sharp peak of the apparent friction coefficient $\gamma_{\mathrm{MD}}(z_s)$. This peak is absent if contributions of the interface modes to the random force are removed. Since the time scale of the interface mode dynamics is comparable to or is larger than the time scale of the solute dynamics near a free energy barrier, it is necessary to consider dynamics of individual interface modes in order to assess the effect of the interface fluctuations on the solute transport. To accomplish this goal, we investigate the free energy landscape of the solute-interface system in more detail.

From Eq. (15) it follows that a minimum energy path (MEP) on the free energy surface $G(z_s;\{\hat{h}_{\mathbf{k}}\})$ is a path such that $\hat{h}_{\mathbf{k}}=\hat{h}_{\mathbf{k}}^{(0)}(z_s)$ for all $\mathbf{k}$ at every solute position z_s along the path. The system free energy on this path, $G_{\mathrm{MEP}}(z_s;\{\hat{h}_{\mathbf{k}}\})=G_0(z_s)$, does not depend on the details of the coupling between the solute and the interface fluctuations and, in order

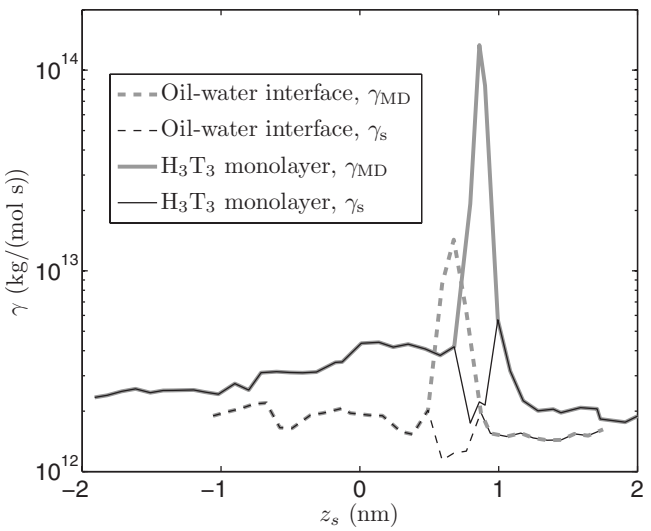

FIG. 7. Solute friction coefficients γ_{MD} and γ_s obtained from the ACF of forces $\Gamma_{\mathrm{MD}}(t;z_s)$ and $\Gamma_s(t;z_s)$ are shown by thick gray and thin black lines, respectively. The friction coefficients at the surfactant-free oil-water interface and H_3T_3 monolayer are shown by dashed and solid lines, respectively.

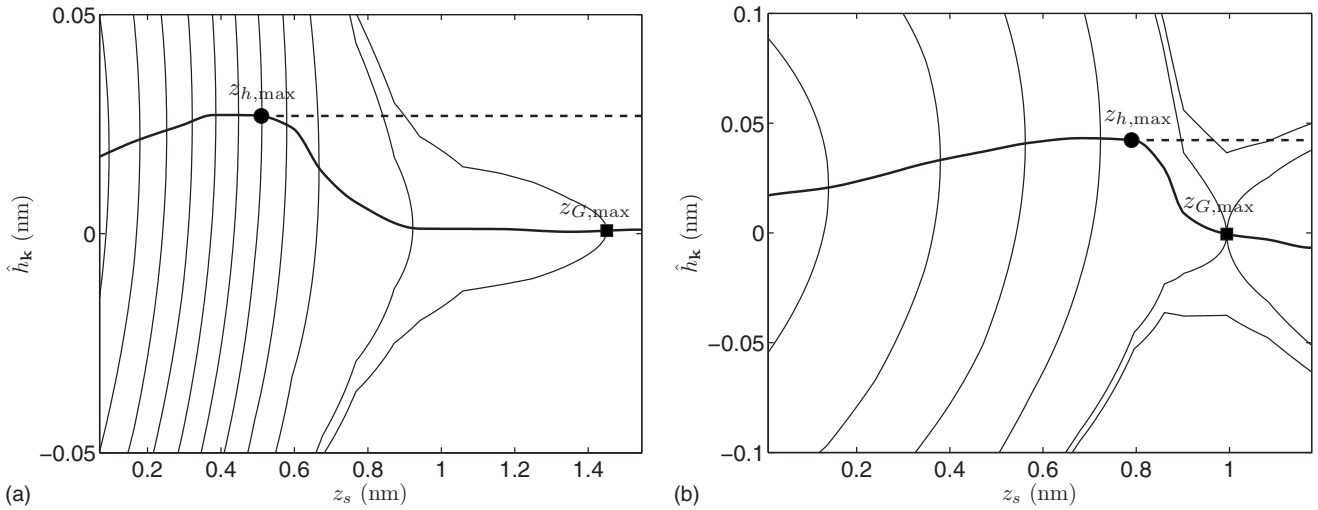

FIG. 8. Projection of the free energy $G(z_s,\{\hat{h}_{\mathbf{k}}\})$ on the plane $z_s-\hat{h}_{\mathbf{k}}$ with $|k|=0.64$ nm^{-1} for (a) surfactant-free oil-water interface and (b) surfactant monolayer. Minimal energy paths are shown by thick solid lines and the paths assumed in the calculation of the mean transport time $T[\gamma_s,\tilde{G}]$ are shown by dashed lines. Points $z_{h,\max}$ corresponding to maxima of $\hat{h}_{\mathbf{k}}^{(0)}(z_s)$ are shown by circles and points $z_{G,\max}$ corresponding to maxima of $G_0(z_s)$ are shown by squares.

to obtain the free energy change and/or barrier associated with the solute transport, it is sufficient to obtain $G_0(z_s)$.

However, the potential of mean force obtained from constrained MD simulations may differ from $G_0(z_s)$. Equations (12) and (15) yield the following expression for the mean force acting on the solute when the latter is constrained at $z=z_s$:

$$\langle F_z(z_s)\rangle|_{z_s=\text{const}} = -\left\langle \frac{dG(z_s;\{\hat{h}_{\mathbf{k}}\})}{dz_s}\right\rangle\Bigg|_{z_s=\text{const}}$$

$$= -G_0'(z_s) - \frac{k_BT}{2}\frac{d}{dz_s}\sum_{\mathbf{k}\neq 0}\ln\alpha_{\mathbf{k}}(z_s). \tag{18}$$

If the dependence of $\alpha_{\mathbf{k}}(z_s)$ on z_s is weak, which is the case for the systems considered in the current work, the potential of mean force obtained from constrained MD simulations closely approximates $G_0(z_s)$ (up to an additive constant). However, dependence of $\alpha_{\mathbf{k}}$ on the solute position is expected to be stronger for larger and/or polar or charged solutes and in these cases one may not be able to neglect the correction to $G_0(z_s)$.

Although the potential of mean force $G_0(z_s)$ along MEP does not depend on the interface configuration, the interface modes may significantly alter MEP geometry near point $z_{G,\max}$ corresponding to the maximum of $G_0(z_s)$. This situation is illustrated in Fig. 8, which shows projections of $G(z_s;\{\hat{h}_{\mathbf{k}}\})$ and MEP on a z_s–$\hat{h}_{\mathbf{k}}$ plane in the region of the strong solute-interface coupling. Once the solute passes point $z_{h,\max}$ corresponding to the maximum of $\hat{h}_{\mathbf{k}}^{(0)}(z_s)$, MEP makes a sharp turn toward $\hat{h}_{\mathbf{k}}^{(0)}=0$. We expect that the observed deviation of MEP from a straight line in an immediate neighborhood of $z_{G,\max}$ is a common feature of transport across flexible interfaces. As discussed in Sec. III, the origin of the sharp decrease of $\hat{h}_{\mathbf{k}}^{(0)}(z_s)$ is disappearance of the interface protrusions once they become energetically unfavorable. Moreover, $z_{h,\max}$ is likely to directly precede the free energy maximum because, once the protrusions disappear, the solute energy is determined only by its interactions with the surrounding unfavorable phase.

Before computing the solute transport rate, let us recall a well-known result for a mean transport time of a particle whose motion is described by a one-dimensional Langevin equation in the high-friction limit [42],

$$T_{a\to b}[\gamma,G] = \frac{1}{k_BT}\int_a^b \gamma(y)e^{G(y)/k_BT}dy\int_a^y e^{-G(z)/k_BT}dz. \tag{19}$$

Here, $G(z)$ is the potential of mean force, $\gamma(z)$ is the friction coefficient, and $T_{a\to b}[\gamma,G]$ is the mean transport time of the particle from $z=a$ to $z=b$.

Equation (19) is directly applicable if the coupling between the solute and interface dynamics is neglected. To take this coupling into account, it is necessary to consider a generalization of Eq. (19) to a stochastic system with multiple degrees of freedom. This can be accomplished, e.g., if the system motion, on average, takes place along MEP. In this case, the integrations are performed along MEP and the system dynamics in directions transversal to MEP is captured by factors corresponding to frequencies of oscillations in these directions. The underlying assumption of this generalization is that the time scale of approach to MEP is much faster than the time scale of motion along MEP.

This assumption fails for the coupled solute-interface dynamics when the solute is located between points $z_{h,\max}$ and $z_{G,\max}$. Due to proximity of these points, the difference between the free energies, $\Delta G\equiv G_0(z_{G,\max})-G_0(z_{h,\max})$, along MEP passing through these points, is small. Specifically, for transport across the surfactant-free interface, ΔG

TABLE I. Mean escape times $T[\gamma, G]$ obtained from Eq. (19) using different approximations to the friction coefficient $\gamma(z_s)$ and the potential of mean force $G(z_s)$.

	$T[\gamma_{MD}, G_0]$	$T[\gamma_s, G_0]$	$T[\gamma_s, \tilde{G}]$
Surfactant-free interface	5.82×10^3 s	1.87×10^3 s	2.40×10^3 s
H_3T_3 monolayer	1.45×10^5 s	2.45×10^4 s	4.13×10^4 s

$=6.3$ kJ/mol and for transport across the H_3T_3 monolayer, $\Delta G=2.5$ kJ/mol. The average contribution of each interface mode to the free energy is $k_BT=2.5$ kJ/mol at $T=300$ K, i.e., the driving force for approach to MEP is comparable with the driving force for motion along MEP between $z_{h,\max}$ and $z_{G,\max}$. In addition, the friction coefficients of the interface modes, $\gamma_{\mathbf{k}}=\tau_{\mathbf{k}}\alpha_{\mathbf{k}}=O(10^{14})$ kg/(mol s), exceed the solute friction coefficient γ_s shown in Fig. 7 by two orders of magnitude. These two observations imply that near $z_{G,\max}$ the change of the interface configuration is much slower than the solute transport. Therefore, the solute will pass through point $z_{G,\max}$ before the protrusion formed when the solute was at $z_{h,\max}$ disappears.

To estimate the effect of the slow interface relaxation on the solute transport rate, we assume that the interface configuration remains unchanged and the system follows the path shown by the dashed line in Fig. 8 for $z_s \geqslant z_{h,\max}$. The change of $\hat{h}^{(0)}_{\mathbf{k}}(z_s)$ with increase of z_s is much more gradual when $z_s \leqslant z_{h,\max}$, see Fig. 6(a). Therefore, we assume that the system moves along MEP when $z_s \leqslant z_{h,\max}$. The free energy along the assumed path is

$$\tilde{G}(z_s)=\begin{cases} G_0(z_s), & z_s \leqslant z_{h,\max}, \\ G_0(z_s)+\dfrac{1}{2}\displaystyle\sum_{\mathbf{k}\neq 0}\alpha_{\mathbf{k}}(z_s)|\hat{h}^{(0)}_{\mathbf{k}}(z_{h,\max})-\hat{h}^{(0)}_{\mathbf{k}}(z_s)|^2, & z_s \geqslant z_{h,\max}. \end{cases} \tag{20}$$

Weak dependence of $\alpha_{\mathbf{k}}(z_s)$ on z_s allows us to neglect changes in frequencies ω_j of the system oscillations in the directions transversal to MEP when $z_s \leqslant z_{h,\max}$. The changes in ω_j can be also neglected for $z_s \geqslant z_{h,\max}$ since the interface is assumed to be frozen on the time scale of the solute motion in this region. These assumptions allow us to estimate the mean time of the solute transport across the interface using Eq. (19) with $\gamma=\gamma_s$ and $G=\tilde{G}$.

The obtained mean transport times $T[\gamma_s, \tilde{G}]$ across the surfactant-free interface and H_3T_3 monolayer are listed in Table I along with transport times obtained if some or all aspects of the coupled solute-interface dynamics are neglected. In the latter case, the system trajectory is assumed to follow MEP, i.e., $G=G_0$ and the solute friction is assumed to be either (i) the apparent friction γ_{MD} obtained directly from constrained MD simulations or (ii) friction γ_s obtained from γ_{MD} by removing the contribution of the interface modes.

The mean transport time $T[\gamma_{MD}, G_0]$ obtained if the solute-interface coupling is completely neglected overestimates the mean transport time due to an overestimate of the friction coefficient. On the other hand, using the corrected friction coefficient γ_s but still assuming motion along MEP leads to an underestimate of the transport time.

In this paper, we considered a coarse-grained model for transport of a small hydrophobic solute across an interface of two immiscible fluids and across a surfactant monolayer. We demonstrated that the main condition for the coupling between the solute and interface dynamics is attraction between the solute and one of the phases separated by the interface. This condition is satisfied in a large number of interfacial systems and therefore the solute-interface coupling is expected to affect transport across most fluid and flexible membranes. The implications of the dynamic solute-interface coupling for transport across the interface are expected to be significant for systems with a strong attraction between a solute and one of the phases separated by the interface.

ACKNOWLEDGMENTS

This research was supported by the National Science Foundation through Grant No. CTS-0500090. Computational resources were in part provided by the University of Florida High-Performance Computing Center.

[1] S. P. Moulik and B. K. Paul, Adv. Colloid Interface Sci. **78**, 99 (1998).
[2] R. P. Bagwe, J. R. Kanicky, B. J. Palla, P. K. Patanjali, and D. O. Shah, Crit. Rev. Ther. Drug Carrier Syst. **18**, 77 (2001).
[3] *Handbook of Microemulsion Science and Technology*, edited by P. Kumar and K. L. Mittal (Marcel Dekker, New York, 1999).
[4] T. F. Vandamme, Prog. Retin Eye Res. **21**, 15 (2002).
[5] C. J. Slevin, J. A. Umbers, J. H. Atherton, and P. R. Unwin, J. Chem. Soc., Faraday Trans. **92**, 5177 (1996).

[6] K. Nakatani, M. Sudo, and N. Kitamura, J. Phys. Chem. B **102**, 2908 (1998).
[7] T. Osakai, A. Ogata, and K. Ebina, J. Phys. Chem. B **101**, 8341 (1997).
[8] T. Sakai, Y. Takeda, F. Mafuné, M. Abe, and T. Kondow, J. Phys. Chem. B **106**, 5017 (2002).
[9] I. Benjamin, Science **261**, 1558 (1993).
[10] M. Hayoun, M. Meyer, and P. Turq, J. Phys. Chem. **98**, 6626 (1994).
[11] K. J. Schweighofer and I. Benjamin, J. Phys. Chem. **99**, 9974 (1995).
[12] A. Pohorille and M. A. Wilson, J. Chem. Phys. **104**, 3760 (1996).
[13] T.-M. Chang and L. X. Dang, Chem. Phys. Lett. **263**, 39 (1996).
[14] T.-M. Chang and L. X. Dang, J. Chem. Phys. **108**, 818 (1998).
[15] P. A. Fernandes, M. N. D. S. Cordeiro, and J. A. N. F. Gomes, J. Phys. Chem. B **103**, 8930 (1999).
[16] P. A. Fernandes, M. N. D. S. Cordeiro, and J. A. N. F. Gomes, J. Phys. Chem. B **104**, 2278 (2000).
[17] M. Lauterbach, E. Engler, N. Muzet, L. Troxler, and G. Wipff, J. Phys. Chem. B **102**, 245 (1998).
[18] H. A. Patel, E. B. Nauman, and S. Garde, J. Chem. Phys. **119**, 9199 (2003).
[19] R. A. Marcus, J. Chem. Phys. **113**, 1618 (2000).
[20] A. A. Kornyshev, A. M. Kuznetsov, and M. Urbakh, J. Chem. Phys. **117**, 6766 (2002).
[21] L. I. Daikhin, A. A. Kornyshev, A. M. Kuznetsov, and M. Urbakh, Chem. Phys. **319**, 253 (2005).
[22] K. J. Schweighofer and I. Benjamin, J. Phys. Chem. A **103**, 10274 (1999).
[23] L. X. Dang, J. Phys. Chem. B **103**, 8195 (1999).
[24] L. X. Dang, J. Phys. Chem. B **105**, 804 (2001).
[25] S. J. Marrink, A. H. de Vries, and A. E. Mark, J. Phys. Chem. B **108**, 750 (2004).
[26] A. Gupta, A. Chauhan, and D. I. Kopelevich, J. Chem. Phys. **128**, 234709 (2008).
[27] G. Mohan and D. I. Kopelevich, J. Chem. Phys. **128**, 044905 (2008).
[28] D. van der Spoel, E. Lindahl, B. Hess, G. Groenhof, A. E. Mark, and H. J. C. Berendsen, J. Comput. Chem. **26**, 1701 (2005).
[29] H. J. C. Berendsen, J. P. M. Postma, W. F. van Gunsteren, A. DiNola, and J. R. Haak, J. Chem. Phys. **81**, 3684 (1984).
[30] J. D. Weeks, J. Chem. Phys. **67**, 3106 (1977).
[31] E. Chacón and P. Tarazona, Phys. Rev. Lett. **91**, 166103 (2003).
[32] P. Tarazona and E. Chacón, Phys. Rev. B **70**, 235407 (2004).
[33] J. Chowdhary and B. M. Ladanyi, J. Phys. Chem. B **110**, 15442 (2006).
[34] B. Roux and M. Karplus, J. Phys. Chem. **95**, 4856 (1991).
[35] S. J. Marrink and H. J. C. Berendsen, J. Phys. Chem. **98**, 4155 (1994).
[36] G. R. Haynes, G. A. Voth, and E. Pollak, J. Chem. Phys. **101**, 7811 (1994).
[37] J. P. Ryckaert, G. Ciccotti, and H. J. C. Berendsen, J. Comput. Phys. **23**, 327 (1977).
[38] S. Nosé, Mol. Phys. **52**, 255 (1984).
[39] W. G. Hoover, Phys. Rev. A **31**, 1695 (1985).
[40] M. Parrinello and A. Rahman, J. Appl. Phys. **52**, 7182 (1981).
[41] S. Nosé and M. L. Klein, Mol. Phys. **50**, 1055 (1983).
[42] G. W. Gardiner, *Handbook of Stochastic Methods for Physics, Chemistry, and the Natural Sciences* (Springer-Verlag, Berlin, 1983).